A numerical study on ice failure process and ice-ship interactions by Smoothed Particle Hydrodynamics

Ningbo Zhang [a], Xing Zheng [a, *], Qingwei Ma [b, a], Zhenhong Hu [a, c]

[a] College of Shipbuilding Engineering, Harbin Engineering University, Harbin, 150001, China
[b] Schools of Mathematics, Computer Science and Engineering, City, University of London, London, EC1V 0HB, UK
[c] State Key Laboratory Coastal and Offshore Engineering, Dalian University of Technology, 116023, China

ABSTRACT

In this paper, a Smoothed Particle Hydrodynamics (SPH) method is extended to simulate the ice failure process and ice-ship interactions. The softening elastoplastic model integrating Drucker-Prager yield criterion is embedded into the SPH method to simulate the failure progress of ice. To verify the accuracy of the proposed SPH method, two benchmarks are presented, which include the elastic vibration of a cantilever beam and three-point bending failure of the ice beam. The good agreement between the obtained numerical results and experimental data indicates that the presented SPH method can give the reliable and accurate results for simulating the ice failure progress. On this basis, the extended SPH method is employed to simulate level ice interacting with sloping structure and three-dimensional ice-ship interaction in level ice, and the numerical data is validated through comparing with experimental results of a 1:20 scaled Araon icebreaker model. It is shown the proposed SPH model can satisfactorily predict the ice breaking process and ice breaking resistance on ships in ice-ship interaction.
© 2019 Society of Naval Architects of Korea. Production and hosting by Elsevier B.V. This is an open access article under the CC BY-NC-ND license (http://creativecommons.org/licenses/by-nc-nd/4.0/).

1. Introduction

To fulfill the requirements of the increasing activities in Arctic regions, numerical simulation of ice-structure interactions is becoming more and more important during the design and operation of the marine structures (Zhou et al., 2013). The ice failure progress during ice-structure interactions is complex. For example, during ice-ship interactions, the failure mode of ice includes the local crushing fracture, shear failure, vertical deflection, bending failure, splitting failure, or mixed failure mode. The bending failure of the ice sheet generally dominates over the other modes of failure (Lubbad and Løset, 2011; Zhou et al., 2018a). Generally, the ice begins to break by forming circumferential and radial cracks. After broken from the ice sheet, the broken ice floes may accelerate, rotate, collide, accumulate or submerge and slide along the hull until they are cleared away. According to overview presented by Valanto (2001), the ship-level ice interaction process can be divided into several phases: breaking, rotating, sliding and clearing. The ice begins to fail with localised crushing at the contact zone. The

crushing force increases until the ice sheet fails as the ship advances and the contact area increases. So far, this subject has received extensive attentions and many relevant studies have been carried out to investigate the ice failure process and predict the ice resistance during the interactions between ice and structures.

Some analytical and empirical approaches have been proposed to predict ice breaking resistance. For example, the analytical equations were proposed by Keinonen et al. (1996) to predict ice resistance for a ship in level ice. More recently, Cho and Lee (2015) proposed a multiple regression analysis method to estimate ice breaking resistance, which considered various influencing factors and included a logical procedure for the ice resistance prediction of ice breaker. Besides, some simplified empirical models were also suggested to calculate the interaction force between the ice and the hull, e.g., the Matlock model (1969). Subsequently, Withalm and Hoffmann (2010) used Matlock model to analyze the interaction between full scale ice and structure, and explored the influences of ice surface variation and structural stiffness. Later, Hu and Zhou (2015) used some empirical methods to calculate ice resistance for icebreaking vessels in level ice. Zhou et al. (2016) presented a method combining numerical simulations and semi-empirical formula to simulate the ship-ice interaction problem solved in the time domain. And more recently, a semi-empirical method

---

* Corresponding author.
  E-mail address: zhengxing@hrbeu.edu.cn (X. Zheng).
  Peer review under responsibility of Society of Naval Architects of Korea.

based on Lindqvist's model was proposed by Jeong et al. (2017), and was further simplified to predict the ship resistance in level ice.

In addition, some numerical methods have also been proposed to predict ice resistance of ship and simulate ice failure progress in ice-ship interactions. Aksnes (2010) proposed a one dimensional numerical model including elastic beam theory with friction theory to study the response of moored ships and interaction force between the hull and the ice. Su et al. (2010) developed a numerical program to predict the ship motion and resistance in uniform level ice based on Lindqvist's ice resistance model (1989). The ice sheet failure and rubble pile formation process against a wide inclined structure were simulated by Paavilainen et al. (2011) using the coupling forms of finite element and discrete element method. Lubbad and Løset (2011) presented a numerical real-time model to simulate the process of ship-ice interaction in level ice. They simulated the progress of a cracking pattern and ice breaking process during ice interaction with the ship hull at the bow area. A numerical model which considers the effect of submersion of broken ice floes is presented to simulate the dynamic ice loads acting on an icebreaking tanker in level ice by Zhou et al. (2013). Zhou et al. (2018b) presented a numerical method to simulate level ice interaction with ship in transverse and longitudinal directions in time domain. Recently, Liu et al. (2018) used the peridynamics to predict ice breaking loads and investigate the ship-ice interaction process in ice rubble. The sliding, rotation and accumulation of broken ice can be simulated in their work.

In recent years, the Smoothed Particle Hydrodynamics (SPH) as a mesh-free approach has been widely applied to computational fluid simulations (Morris et al., 1997; Shao and Lo, 2003; Zheng et al., 2014; Zheng et al., 2017; Gotoh and Khayyer, 2018). Recently, SPH method has also been extended to solve fluid solid interaction problems including the combination plastic and brittle fracture behavior of plates under the water impact (Eghtesad et al., 2012), the fluid flow interactions with saturated porous media (Khayyer et al., 2017), the fluid-elastic solid interactions (Khayyer et al., 2018) and the failure process of a flexible oil boom under the action of combined waves and currents (Shi et al., 2018). In addition, because of its Lagrangian nature, the SPH can be effectively used to the large deformation and failure behavior of solids (Libersky and Petschek, 1991; Benz and Asphaug, 1995; Randles and Libersky, 1996; Bui et al., 2008; Deb and Pramanik, 2013; Zhang et al., 2017). So far, the failure model of soil and rock mechanics by using the SPH have been widely investigated except for the ice. In this paper, the SPH method will be applied to simulate the ice failure process and ice-ship interactions in level ice. The failure model including the elastoplastic constitutive model coupling the Drucker-Prager yield criterion has been integrated to the SPH to simulate the plastic failure of ice.

During the ship-ice interaction, bending are the most dominating failure modes for thin ice floe (Lubbad and Løset, 2011; Zhou et al., 2018a). And ice is a strain-rate-dependent material. If at low strain rate, ice has ductile behavior. It mainly failures in creep and micro-cracking mode and can be treated as a viscous elastic material (Jordaan, 2001). At high strain rates, ice exhibits the typical brittle failure mode (Schulson, 1997, 2001; Schulson and Duval, 2009). In reality, during ice-ship interactions, ice collides with ship at relatively high speeds and correspondingly the ice is at high strain rates (Jordaan, 2001; Gao et al., 2015), which means the ice shows the typical brittle failure mode like bending failure under ships (Schulson, 2001). Therefore, the visco-plastic effect is considered not strong and it is reasonable to use the elastic-plastic constitutive material model to model ice for the simulation of ice-ship interaction in this paper. Nevertheless, more accurate model, such as visco-elastic-plastic, should be considered in the future study.

Although the failure model for ice used in this paper is similar to that in Zhang et al. (2017). Unlike the study on some simple and typical failure modes in Zhang et al. (2017), the main purpose of this paper is to investigate the complex process during the ship-ice interaction and predict ship resistance in level ice. The main contribution of this paper lies in the following two aspects. On the one hand, a simple and effective boundary condition for modeling the contact between ship and ice has been implemented in the SPH framework to simulate the ice-ship interaction. In this method, when simulating the ice-ship interaction, the solid boundary particles representing the ship boundary act as dummy particles to approximate the boundary conditions for ice particles. The introduced method can achieve simple processes for ship-ice interaction even with complex geometries of ship boundary, which can be extended to more complex and practical ice-structure interaction problems. On the other hand, a simple prediction method for ship resistance in level ice is presented in the proposed SPH method. The satisfactory performance in predicting ice resistance prediction is demonstrated by the robust comparisons between the numerical results and experimental data.

The proposed SPH method will be validated through simulating three-point bending failure of ice beam. Then the validated SPH method is extended to simulate level ice interacting with sloping structure and three-dimensional ice breaking process of the icebreaker in level ice. The numerical results of the presented SPH are compared with the ones of the laboratory measurements.

2. Governing equations

The governing equations in a SPH method are the mass and momentum conservation equations written in the Lagrangian form, which are shown as following.

$$\frac{D\rho}{Dt} = -\frac{1}{\rho} \frac{\partial v^\alpha}{\partial x^\alpha} \tag{1}$$

$$\frac{Dv^\alpha}{Dt} = \frac{1}{\rho} \frac{\partial \sigma^{\alpha\beta}}{\partial x^\beta} + g^\alpha \tag{2}$$

where α and β indicate the Cartesian components in x and y directions; ρ, v and $\sigma^{\alpha\beta}$ are the particle density, velocity and tress tensor, respectively; g is the gravitational acceleration; D/Dt denotes the particle derivative.

$$\sigma^{\alpha\beta} = -p\delta^{\alpha\beta} + s^{\alpha\beta} \tag{3}$$

in which Kronecker delta $\delta^{\alpha\beta} = 1$ if $\alpha = \beta$ or $\delta^{\alpha\beta} = 0$ when $\alpha \neq \beta$. The hydrostatic pressure is defined by the ice constitutive equation using the mean stress, which means $p = -\sigma^{\gamma\gamma}/3$. Hence, the stress tensor can be written as

$$\sigma^{\alpha\beta} = \frac{1}{3}\sigma^{\gamma\gamma}\delta^{\alpha\beta} + s^{\alpha\beta} \tag{4}$$

3. SPH formulations

3.1. Spatial derivatives and particle approximation in SPH

In SPH method, the quantities of particle i can be approximated by the direct summation of the relevant quantities of its neighbouring particles j. The continuity Eq. (1) can be approximated as follows:

$$\frac{D\rho_i}{Dt} = m_i \sum_{j=1}^{N} \frac{m_j}{\rho_j} \left(v_i^\alpha - v_j^\alpha \right) \frac{\partial W_{ij}}{\partial x_i^\alpha} \qquad (5)$$

where ρ_i and m_i are the density and mass of particle i with velocity component v_i; ρ_j and m_j are the density and mass of particle j which has velocity component v_j.

An artificial stress method proposed by Monaghan (2000) and Gray et al. (2001) is used in this paper to remove numerical instability (Swegle et al., 1995) caused by clumping of the SPH particles when SPH is applied to solid. The SPH approximation of the momentum equation for ice model is

$$\frac{dv_i^\alpha}{dt} = \sum_{j=1}^{N} m_j \left(\frac{\sigma_i^{\alpha\beta}}{\rho_i^2} + \frac{\sigma_j^{\alpha\beta}}{\rho_j^2} - \Pi_{ij} \cdot \delta^{\alpha\beta} + f_{ij}^n \left(R_i^{\alpha\beta} + R_j^{\alpha\beta} \right) \right) \frac{\partial W_{ij}}{\partial x_i^\beta} + g^\alpha$$

$$(6)$$

where $R_i^{\alpha\beta}$ and $R_j^{\alpha\beta}$ are the artificial stress tensor of particles i and j, respectively, with the correction parameter $\varepsilon = 0.3$; $n = 4$ for all tests discussed in this study; and f_{ij} is defined as $f_{ij} = W_{ij}/W(\Delta d, h)$, Δd is the initial distance between particles. In this paper, the cubic B-spline kernel proposed by Monaghan and Lattanzio (1985) is used.

In addition, the position of particle i is defined based on the XSPH method (Monaghan, 1992), as

$$\frac{Dx_i^\alpha}{Dt} = v_i^\alpha + \bar{\varepsilon} \sum_{j=1}^{N} \frac{m_j}{\rho_j} \left(v_j^\alpha - v_i^\alpha \right) W_{ij}, \quad \bar{\varepsilon} \in [0, 1] \qquad (7)$$

where the parameters $\bar{\varepsilon} = 0.1$ is used in this study.

3.2. SFDI method

The Simplified Finite Difference Interpolation (SFDI) method is used to calculate the strain rate of the ice particles to improve the accuracy in the original SPH, more details about SFDI method can be found in Ma (2008). The strain rate of the tensor by SFDI method in 2D case can be written as:

$$\dot{\varepsilon}^{\alpha\beta} = \frac{1}{2} \left(\sum_{j=1,j\neq i}^{N} \frac{n_{i,\alpha}B_{ij,\beta} - n_{i,\beta}B_{ij,\alpha}}{n_{i,x}n_{i,y} - n_{i,\alpha\beta}^2} \left(v_j^\alpha - v_i^\alpha \right) \right.$$
$$\left. + \sum_{j=1,j\neq i}^{N} \frac{n_{i,\beta}B_{ij,\alpha} - n_{i,\alpha}B_{ij,\beta}}{n_{i,x}n_{i,y} - n_{i,\alpha\beta}^2} \left(v_j^\beta - v_i^\beta \right) \right) \qquad (8)$$

where $n_{i,m} = \sum_{j=1,j\neq i}^{N} \frac{(r_j^m - r_i^m)^2}{|r_j - r_i|^2} W(r_{ij})$, $n_{i,mk} = \sum_{j=1,j\neq i}^{N} \frac{(r_j^m - r_i^m)(r_j^k - r_i^k)}{|r_j - r_i|^2} W(r_{ij})$, $B_{ij,m} = \frac{(r_j^m - r_i^m)}{|r_j - r_i|^2} W(r_{ij})$, where $m = x, k = y$ or $m = y, k = x, N$ is the number of neighboring particle for particle i, r_j^m indicates the component of the position vector of x or y direction.

3.3. Boundary conditions and ship boundary treatments

In this paper, the wall boundaries are modeled by the particles similar to Adami et al. (2012), which prevent inner real ice particles from penetrating the wall. For the ice-ship interactions, the ship boundary is also modeled by the particles, which is shown in Fig. 1. The boundary particles on the hull surface should be dense enough to prevent the ice particles from penetrating the solid wall boundary. When solving the ice domain equations, the boundary
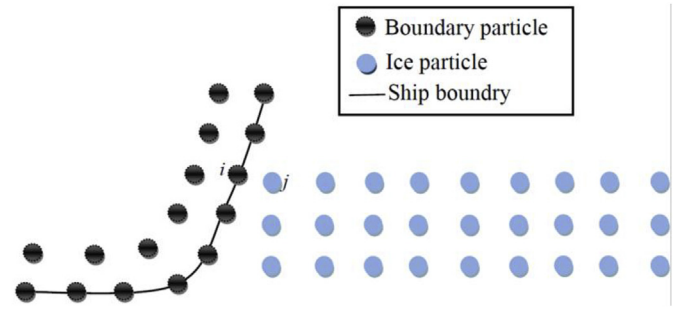

Fig. 1. A schematic diagram of ship boundary treatment.

particles in the computational domain of the ice particle also act as dummy particles for imposing boundary conditions.

These boundary particles contribute to the continuity and momentum equation in the ice phase to make the continuity of stress and velocity be satisfied for the real ice particles near the boundary. And these boundary particles have the same velocity as the physical boundary and their density is set equal to reference density. When using boundary particles as dummy particles to approximate the interface between the ship boundary and ice, the stresses of these particles have to be calculated from the ice to accurately approximate the stress gradient in the ice phase near the boundary. And the stresses of these boundary particles are calculated by using the interpolation over neighboring ice particles similar to Adami et al. (2012) (Fig. 1), i.e.,

$$\sigma_i^{\alpha\beta} = \frac{\sum_{j=1}^{N} \sigma_j^{\alpha\beta} W_{ij}}{\sum_{j=1}^{N} W_{ij}} \qquad (9)$$

where $\sigma_i^{\alpha\beta}$ is the stress of the particle i on the solid boundary, j is the index of its neighboring ice particles, N is the neighbor particle number of the support domain of wall boundary particle i.

In addition, the free-slip boundary condition is also applied by simply neglecting the viscous interaction between ice particles and adjacent solid boundary particles. The main advantage of this boundary method is its simplicity in computation, since it does not need complex computations for the ship boundary and interface surface information.

Similar to the study in Bouscasse et al. (2013) where the wave interaction with floating bodies is simulated, when ship boundary particles act as dummy particles for the ice phase, the approximations of the force on the ship from the ice particles is evaluated by using the volume integration of the stresses tensor of its neighboring ice particles. So, in the present case, the force on ship boundary from ice particles can be derived as

$$\mathbf{F}_{ice-shipboundary} = \sum_{i \in boundary}^{N} m_i \sum_{j \in ice}^{N} m_j \left(\frac{\boldsymbol{\sigma}_i}{\rho_i^2} + \frac{\boldsymbol{\sigma}_j}{\rho_j^2} \right) \nabla_i W_{ij} \qquad (10)$$

4. Failure model for ice in the SPH framework

In this paper, an elastoplastic model based on Deb and Pramanik (2013) is introduced to SPH to simulate the ice failure behavior, which is briefly introduced in this paper. A more thorough presentation of this elastoplastic model can be found in Deb and

Table 1
Summary of the main contents of the elastoplastic model.

Main stages	Main methods	Main formulas
The elastic predictor	The elastic stress rate of the tensor is calculated by the generalized Hooke's law as follows: (7)	$\dot{\sigma}^{\alpha\beta} = 2G\dot{e}^{\alpha\beta} + K\dot{\varepsilon}_{ev}^{\gamma\gamma}\delta^{\alpha\beta}$ in which α and β are free indexes;
The yield criterion	According to Drucker–Prager yield criterion, when yield function $F(\sigma^{\alpha\beta},c) \leq 0$, the problem is elastic stage, else it is in plastic flow regime.	$F(\sigma^{\alpha\beta},c) = \sqrt{J_2(s^{\alpha\beta})} + \eta I_1(\sigma^{\alpha\beta}) - \xi c = 0 Q(\sigma^{\alpha\beta},c) = \sqrt{J_2(s^{\alpha\beta})} + \overline{\eta}I_1(\sigma^{\alpha\beta})$
The plastic corrector	When $F(\sigma^{\alpha\beta},c) > 0$, plastic correction is required. The goal is to bring the stress tensor back to the yield surface.	$\sigma^{\alpha\beta} = \begin{cases} (I_1 - K\Delta\varepsilon_{vp})\delta^{\alpha\beta} & if \ (\sqrt{J_2} - G\Delta\lambda) < 0 \\ \left(1 - \dfrac{G\Delta\lambda}{\sqrt{J_2(s^{\alpha\beta})}}\right)s^{\alpha\beta} + (I_1(\sigma^{\alpha\beta}) - K\overline{\eta}\Delta\lambda)\delta^{\alpha\beta} & else \end{cases}$ where plastic multipliers solved as: $\tilde{F}(\Delta\lambda) = \sqrt{J_2(s^{\alpha\beta})} - G\Delta\lambda + \eta(I_1(\sigma^{\alpha\beta}) - K\overline{\eta}\Delta\lambda)$ $\quad - \xi c(\overline{\varepsilon}_p + \xi\Delta\lambda) = 0$
Cohesion softening	The cohesion softening law is adopted to simulate the reduction of the ice strength numerically.	$c = \begin{cases} c_0 - k\overline{\varepsilon}_p & if \ c > c_R \\ c_R & otherwise \end{cases} \dot{\overline{\varepsilon}}_p = -\dot{\lambda}\dfrac{\partial F}{\partial \kappa} = \dot{\lambda}\xi$

Pramanik (2013). The main contents of this elastoplastic model are given in Table 1.

where the strain rate are given by $\dot{\varepsilon}^{\alpha\beta} = \frac{1}{2}\left(\frac{\partial v^{\alpha}}{\partial x^{\beta}} + \frac{\partial v^{\beta}}{\partial x^{\alpha}}\right)$. The discrete form in SPH of the strain rate can be seen in Eq. (8). In equation of stress rate for the elastic predictor, $\dot{e}^{\alpha\beta} = \dot{\varepsilon}^{\alpha\beta} - \frac{1}{3}\dot{\varepsilon}_{ev}^{\gamma\gamma}\delta^{\alpha\beta}$ is the deviatoric shear strain rate tensor, $\dot{\varepsilon}_{ev}^{\gamma\gamma}$ is the rates of the volumetric parts of the elastic strain tensor, $K = E/(3(1 - 2v))$ is the elastic bulk modulus, $G = E/(2(1 + v))$ is the shear modulus, E is the shear modulus and Young's modulus and v is the Poisson's ratio. In equation of yield function, c is the cohesion of ice, $J_2(s^{\alpha\beta})$ is the second invariant of stress tensor, and $I_1(\sigma^{\alpha\beta})$ is one third of the first invariant of the stress tensor. The parameters η and ξ are defined as $\eta = \frac{6\sin\phi}{\sqrt{3}(3-\sin\phi)}$, $\xi = \frac{6\cos\phi}{\sqrt{3}(3-\sin\phi)}$ where ϕ is the friction angle. In the nonassociated plastic potential function $Q(\sigma^{\alpha\beta},c)$ used to define the relationship between stress and strain, the parameter $\overline{\eta}$ depends on the dilatancy angleφ, and is given by $\overline{\eta} = \frac{6\sin\varphi}{\sqrt{3}(3-\sin\varphi)}$. The volumetric plastic strain increment $\Delta\varepsilon_{vp}$ in the equation of plastic corrector can be computed by solving the following expression: $c\left(\overline{\varepsilon}_p + \frac{\xi}{\eta}\Delta\varepsilon_{vp}\right)\frac{\xi}{\eta} - I_1(\sigma^{\alpha\beta}) + K\Delta\varepsilon_{vp} = 0$. In equation of cohesion softening, k is the specific softening coefficient and c_R is the minimum cohesion, and $\overline{\varepsilon}_p$ is the accumulated plastic strain.

The framework of the SPH program for simulation of ice failure process and ice-ship interactions is schematically described in the flowchart in Fig. 2. At the beginning, the parameters for ice particles including the positions, properties and velocities are initialized. Then the main computational routine is executed according to the sequential flow in Fig. 2.

5. Numerical simulations

In this section, the elastic vibration of a cantilever beam is conducted firstly to verify the feasibility of the presented SPH method. Then the three-point bending of ice beam test is carried out to demonstrate the effectiveness of the presented SPH method for simulating the failure progress of ice. Lastly, it is employed to model the ice-ship interactions in the level ice, and the numerical results are compared with the experimental data.
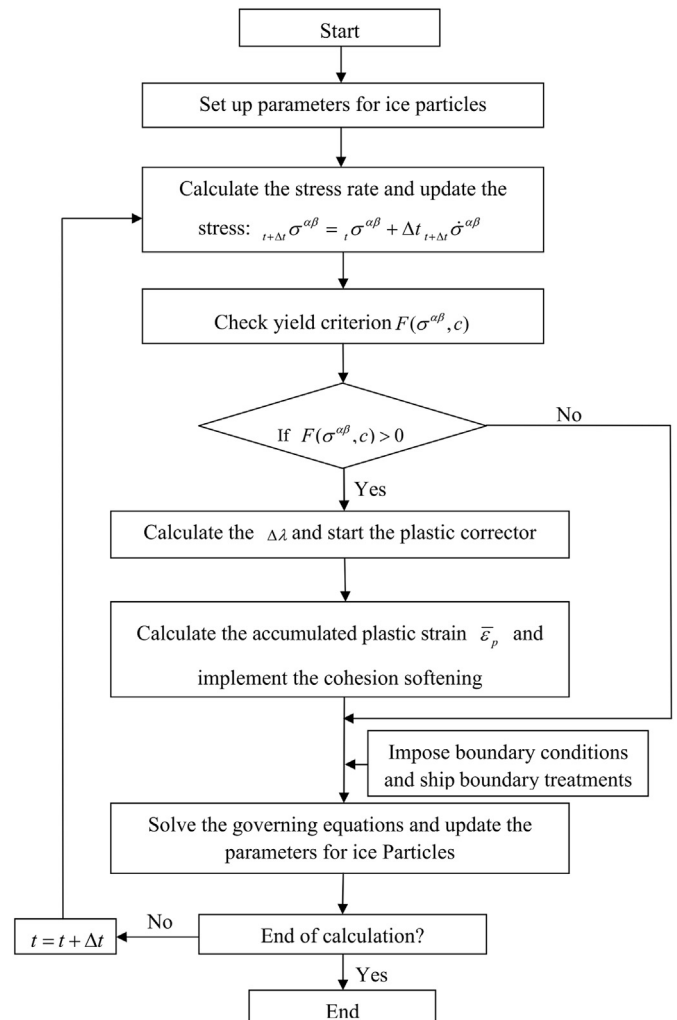

Fig. 2. Framework of the SPH program including the elastic-plastic ice model.

5.1. Elastic vibration of a cantilever beam

In this part, the elastic vibration of a cantilever beam is used as a benchmark test to verify the reliability of the SPH model for the application in solid mechanics. The initial calculation model is
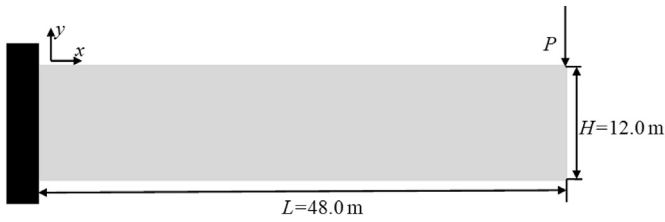
Fig. 3. The cantilever beam and the dynamic loads.

shown in Fig. 3. The elastic modulus E and the Poisson's ratio v of the beam is 3.0×10^7 GPa and 0.3, respectively. External excitation force P is a function of time.

In order to verify the model, a transient load $P = \begin{cases} 1000.0 & t \leq 0.5s \\ 0.0 & t > 0.5s \end{cases}$ is considered. The comparisons of the time histories of the displacement in y direction of the free end of the cantilever beam (h_y), which includes the SPH results (the total number of particle $N = 10000$) and the finite element method (FEM) solutions (Long, 2014) is presented in Fig. 4, in which excellent consistence is observed.

In order to show the convergence properties of the present SPH method, Fig. 5(a) gives the time histories of the vertical displacement h_y, of which each line represents a case by using different particle number N. The convergence test on horizontal
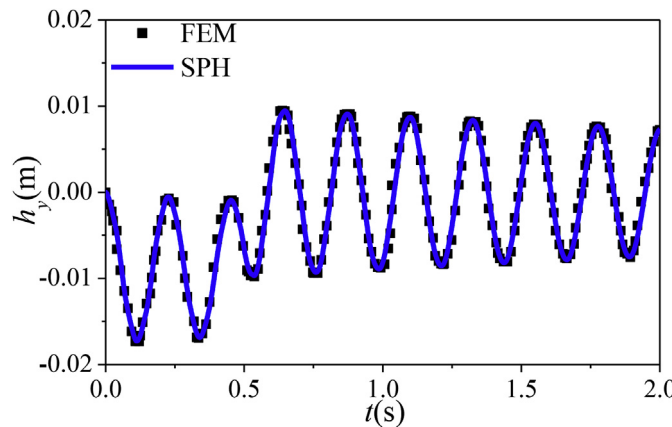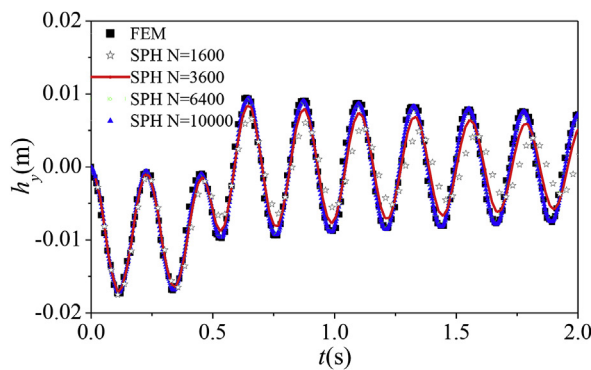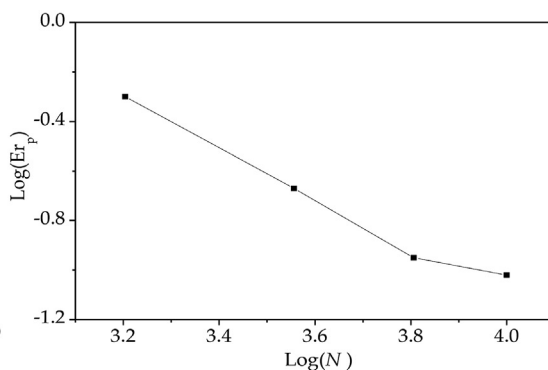

Fig. 4. The time histories of displacement h_y under a transient load.

displacement is shown in Fig. 5(b). The averaged errors of different methods are calculated by $Er_p = \sqrt{\sum_{i=1}^{N}(h-h_0)^2} / \sqrt{\sum_{i=1}^{N}h_0^2}$, where h is the displacement of SPH with different particle numbers from $t = 0.0$ s to $t = 2.0$ s, h_0 is the displacement of experimental data from $t = 0.0$ s to $t = 2.0$ s. It is shown in Fig. 5(a) that as N increases, the results become closer to the experimental data, and when $N \geq 6400$, the differences between that of the FEM become indistinguishable. It could also conclude from Fig. 5(b) that the error of results decreases as the particle number increases. These indicate the convergence of the presented SPH method in the spatial domains.

The validation cases above indicate that the presented SPH model in this paper can be effectively used for simulating solid mechanics problems.

5.2. Three-point bending of ice beam

The sea ice three-point bending experiment was conducted by Ji et al. (2011), in which the bottom of the beam were fixed on two bearings 0.6 m apart and a point load in the middle on the top of the ice beam was applied. The beam is $L = 0.75$m in length and $H = 0.07$m in height. To simulate such a case by using the SPH, the upper and lower bearings are modeled with particles, as shown in Fig. 6, where the ice beam consists of 2768 particles. The downward velocity of the upper bearing is 0.00015 m/s. The ice beam features elastic modulus $E = 1.7$ GPa, the cohesion $c = 0.58$ MPa and the friction angle is $36°$. The dilatancy angle φ in the non-associative plastic rule is set to be one-third of the friction angle, $\varphi = \phi/3$.

Fig. 7(a) gives the snapshot of the experimental results when the ice beam failed. Fig. 7(b)-(d) depicts the potential fracture patterns predicted by the SPH using non-associative flow rule at different time. As shown in Fig. 7(b), the fracture crack obviously occurs at the lower area of the moving bearing and the ice beam breaks into two sections which is in good consistency with the theoretical and experimental results (Ji et al., 2011). The crack subsequently widens and the two sections of the ice beam after failure sink downward as shown in Fig. 7(c). As the upper bearing further moves down, the crack in the ice beam widens and eventually breaks completely to two sections as shown in Fig. 7(d). It should be pointed out that slight crushing failure of the beam at the place in contact with the lower two fixed bearings occurs in SPH simulation, which is also observed in laboratory and understandable.

In order to demonstrate the accuracy of numerical results by using the SPH method, Fig. 8(a)-(b) show a comparison of stress-

(a)

(b)

Fig. 5. Convergence test of the vertical displacement of beam: (a) The time histories of vertical displacement with different particle numbers; (b) Convergence tests of vertical displacement.
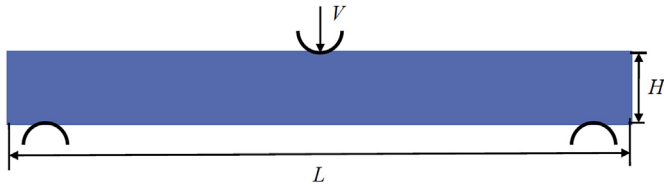
Fig. 6. The sketch of the ice beam model.

time and stress-deflection relationship between the SPH results and the experimental data (Ji et al., 2011), respectively. It is evident that the numerical results of SPH agree very well with the experimental data, which implies that the present SPH model can give accurate results for simulating the ice failure problem.

5.3. Level ice and downward sloping structure interaction

In this apart, the major interaction processes level ice and downward sloping structure are investigated. The bending failure mode of level ice against the inclined structure is observed. The accumulation and rolling of failed ice rubble are also simulated and
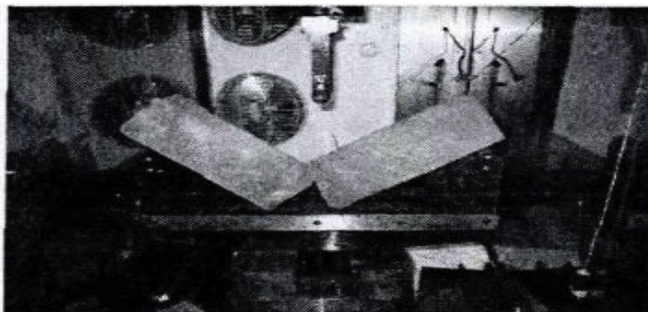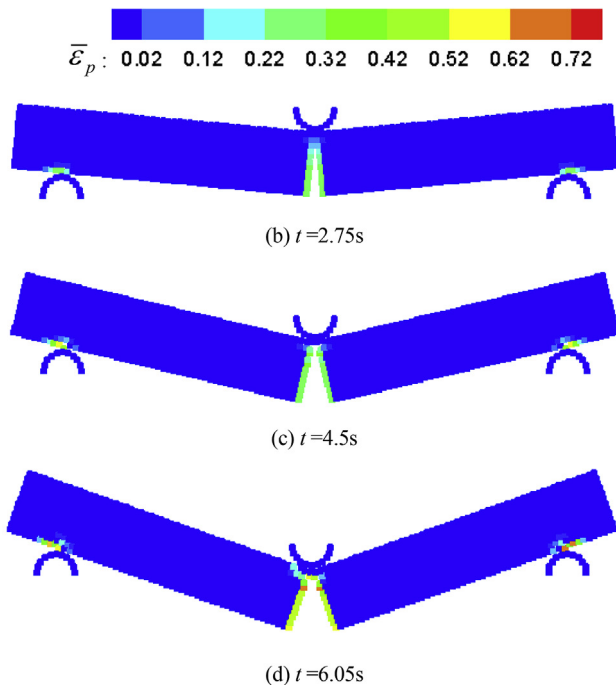

(a) The snapshot in laboratory

$\overline{\varepsilon}_p$: 0.02 0.12 0.22 0.32 0.42 0.52 0.62 0.72

(b) t =2.75s

(c) t =4.5s

(d) t =6.05s

Fig. 7. Snapshots of the ice beam in three-point bending experiment: (a) Laboratory (Ji et al., 2011); (b)–(d) by SPH at different time.
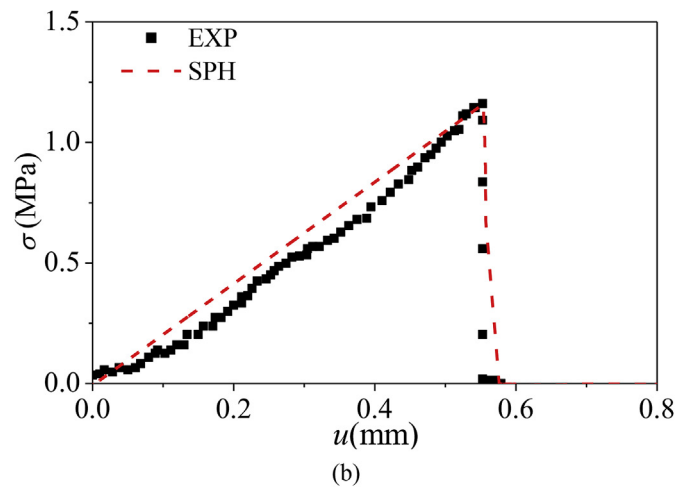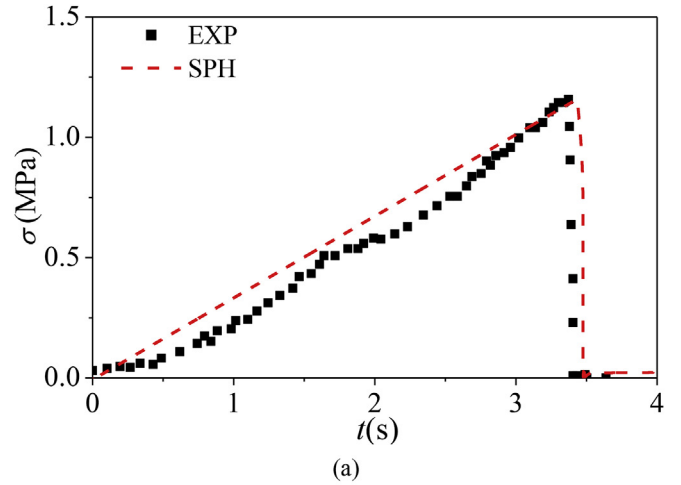

(a)

(b)

Fig. 8. Comparisons between SPH results with laboratory data for the three-point bending experiment: (a) stress against time; (b) stress against deflection.
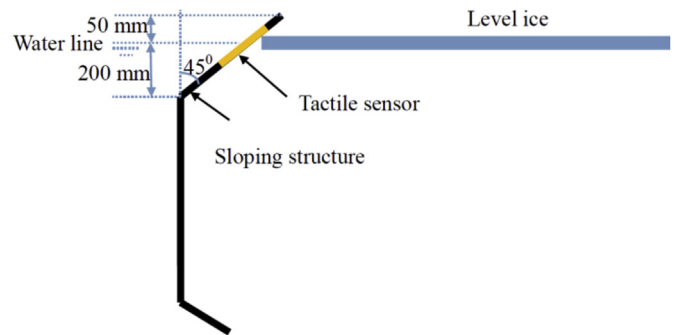

Fig. 9. The schematic setup of sloping structure and level ice.

compared with the experimental observations in Lu et al. (2013). The initial calculation model is shown in Fig. 9. The ice properties including the elastic modulus E, the flexural strength σ_b and ice thickness H as well as the moving speed V of the slope structure are the same with those in the model test (Lu et al., 2013).

At the initial time, the balance of gravity and buoyancy for level ice formation is considered to be satisfied. In this study, the buoyancy acting on level ice is approximately obtained on the particle's position. The buoyancy f_i for ice particle i can be written as

$\overline{\varepsilon}_p$: 0 0.1 0.2 0.3 0.4 0.5 0.6 0.7 0.8 0.9 1

(a) $t = 0.525$ s

(b) $t = 13.125$ s

(c) $t = 22.925$ s
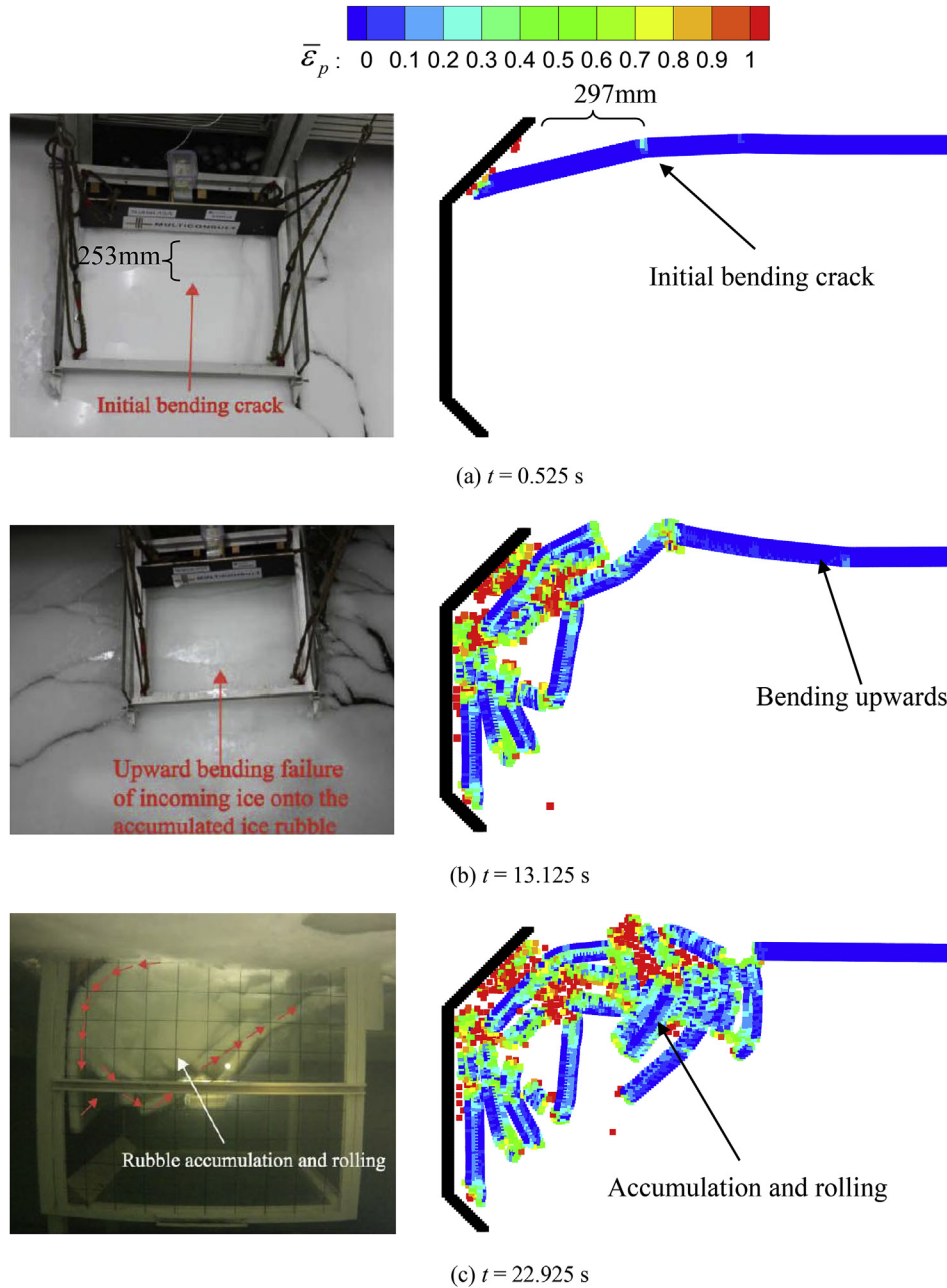
Fig. 10. Comparisons of the failure progress of level ice against sloping structure between laboratory photographs (Lu et al., 2013) (left) and SPH particle snapshots (right) (contours of accumulated plastic strain).

$$f_i = \begin{cases} \rho_w\, g\Delta v & \text{if } i \text{ is completely below the waterline} \\ \rho_w\, g\Delta w & \text{else} \end{cases}$$

(11)

where ρ_w is the water density, Δv is the whole volume of a particle and Δw is the volume of ice particle submerged in water.

Fig. 10 shows a series of the comparison of the failure process of level ice against sloping structure between the numerical results and experimental photographs from Lu et al. (2013) at different time. It can be found in Fig. 10(a) that as the downward sloping plate interacted with the level ice, ice begins to break with the bending crack. In SPH result, the distance of the initial bending crack from the forefront of the sloping structure is 297 mm, which

is approximate to that in the experimental data (about 253 mm) although there are some differences. And the level ice fails by progressively bending downwards as sloping structure advanced. Then some ice rubbles accumulate in front of the structure. Driven by the sloping structure, these accumulated ice rubbles continue to move forward. Under the influence of these accumulated ice rubbles, the failure pattern of the level ice has been transformed from 'bending downwards by the sloping structure' to 'bending upwards by the accumulated ice rubbles' as shown in Fig. 10(b). As the sloping structure continues to move, more broken ice rubbles rotate downwards and then pile up under water shown in Fig. 10(c).

According to the results of Fig. 10, the overall behaviors including the bending failure of ice sheet, the roating and accumulation of broken ice rubbles from our SPH results are similar to
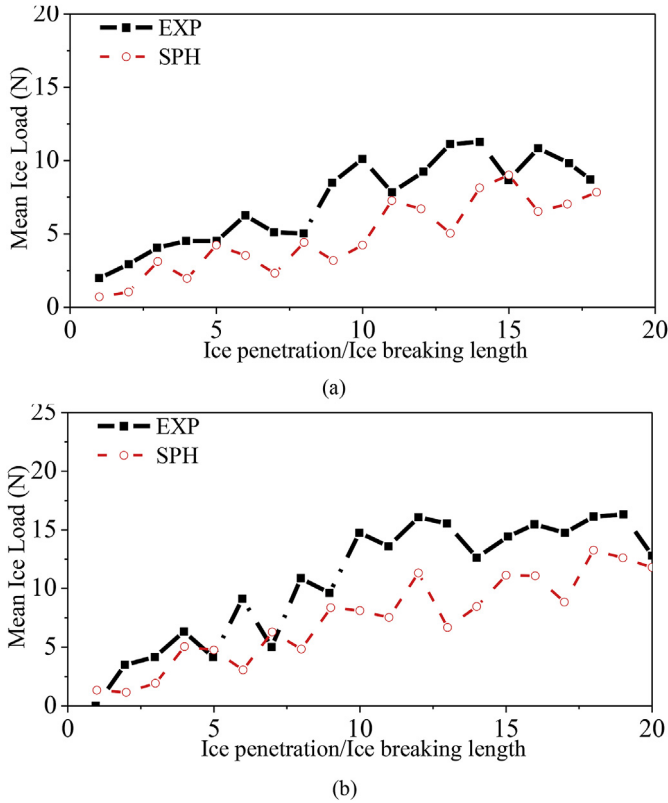
(a)

(b)

Fig. 11. Comparison of temporal variation of horizontal ice load between SPH results and laboratory data: (a)$E = 61$ MPa,$\sigma_b = 53$ kPa, $H = 0.04$ m, $V = 0.045$ m/s; (b)$E = 31$ MPa,$\sigma_b = 47.1$ kPa, $H = 0.04$ M, $V = 0.045$ m/s.
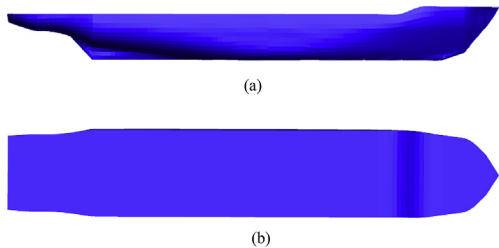

(a)

(b)

Fig. 12. The 3D model of icebreaker Araon: (a) side view; (b) top view.

Table 2
Parameters for full scale and model scale of icebreaker Araon.

Parameters	Full scale	Model scale
Overall Length (m)	107.2	5.36
Breadth (m)	19.0	0.95
Draft (m)	6.8	0.34

that in experimental photos. The good agreement shows that the presented SPH method can be effectively applied to the simulation of level ice and downward sloping structure interaction problems.

In addition, to validate the capability of the presented SPH model in the ice load prediction, the time history of the mean horizontal ice load has been sectionalised and compared between the SPH results and experimental data in Fig. 11. According to the work in Lu et al. (2013), the ice loading history is sectionalised by the ice breaking length. More details about the section and the ice breaking length can be found in Lu et al. (2013). In Fig. 11, our two-
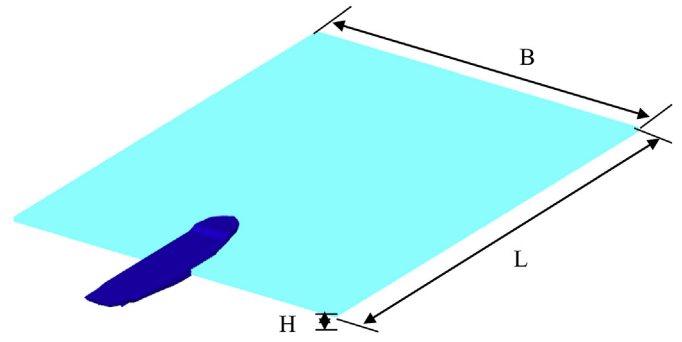

**Fig. 13.** Configuration of the initial condition.

dimensional results are multiplied by the number of the column of the tactile sensor used in Lu et al. (2013). It can be seen that the general trend of the mean ice load is increasing from small load to a certain degree of high load over time. In addition, the ice load jumps down at some sections during the interaction and then rises up at next sections. The underestimation for the ice load can be found in our SPH results in Fig. 11. The main reason may be that the real effect of water is not considered. In our simulation, the fluid buoyancy in vertical direction is considered only. In fact, the water also has horizontal resistance on the accumulated ice rubbles, which may cause the increase of ice load on the sloping structure. In addition, the uneven distribution of ice properties in nature and the complexity of the ice and structure interactions may also led to the underestimation. In general, the increasing trends are in good agreement with that in the model test, even though there are some differences, which signifies the applicability of the presented SPH model.
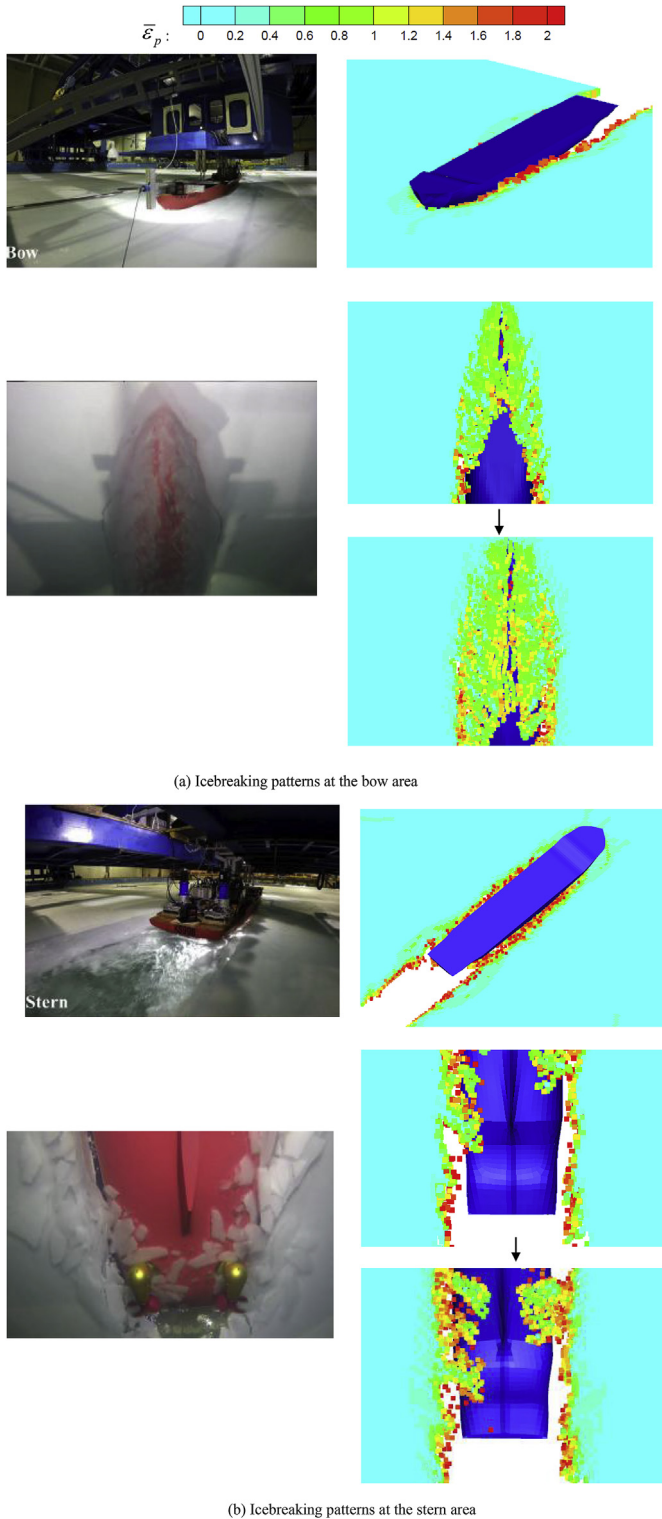
5.4. Ice-ship interaction

In this part, a three dimensional case of level ice failure process by an icebreaker is considered, and the ice resistance on the icebreaker in different working conditions are estimated. The Korean icebreaker Araon (Lau and Akinturk, 2011) is used and the scale 1:20 is employed in numerical simulation. The ship hull based on the drawing of the icebreaker Araon in (Cho et al., 2013) and represented by the solid particles is displayed in Fig. 12. In addition, the parameters of icebreaker Araon in full-scale and model-scale are shown in Table 2. The initial condition of the computation model is illustrated in Fig. 13, where the level ice is $L = 12.0$ m in length, $B = 9.0$ m in width and two thicknesses $H = 0.04$ m and 0.06 m are considered. The level ice is fixed and still initially. The effects of the icebreaker velocity are also investigated, which is the same with that in (Lau and Akinturk, 2011). The buoyancy acting on level ice can be seen in Eq. (11). Although the effects of water phase are not considered in this study, the comparison of some results is still reasonable, such as the pattern of the failure and ice breaking resistance.

Other parameters required for the numerical simulation are also listed here, e.g., the density of ice $\rho = 879.0$ kg/m^3 and the cohesion $c = 12.5$ kPa for ice thickness $H = 0.04$ m, while the density $\rho = 864.0$ kg/m^3 and the cohesion $c = 17.0$ kPa for ice thickness $H = 0.06$ m, which are the same with those in the model test (Lau and Akinturk, 2011). In addition, the elastic modulus $E = 25.0$ MPa, the friction angle is $22.5°$, and the dilatancy angle φ in the non-associative plastic rule is set to be one-third of the friction angle $\varphi = \phi/3$.

Fig. 14 depicts the ice breaking pattern predicted by the SPH. It can be seen that the crushed ice is squeezed to both sides and an

V_x: -0.1   -0.04   0.02   0.08   0.14   0.2   0.26   0.32   0.38   0.44   0.5

(a) $t = 6.0$ s

(b) $t = 8.0$ s
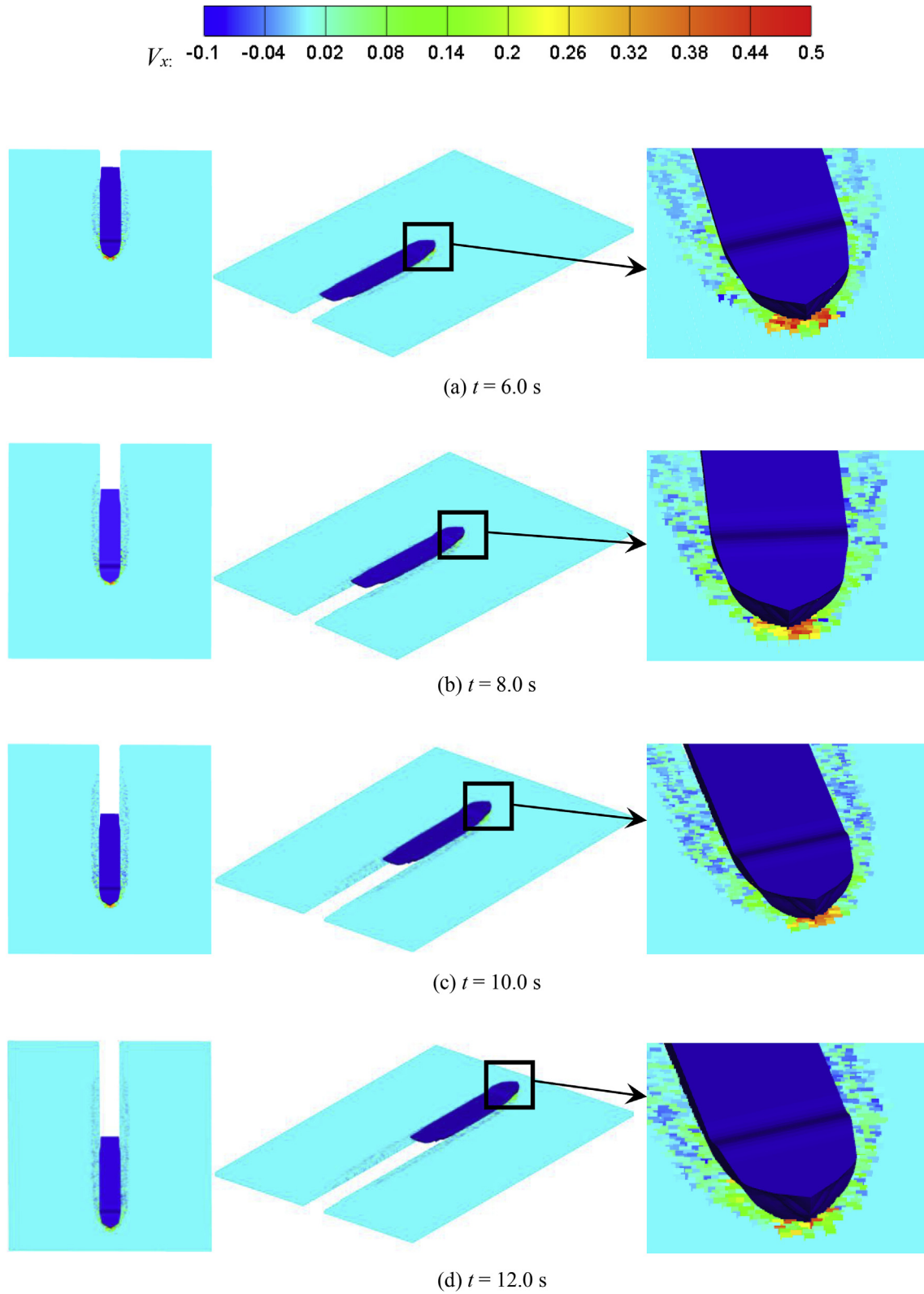
(c) $t = 10.0$ s

(d) $t = 12.0$ s

Fig. 14. Snapshots of ice breaking patterns by SPH at different time: (a) $t = 6.0$ s; (b) $t = 8.0$ s; (c) $t = 10.0$ s; (d) $t = 12.0$ s.

(a) Icebreaking patterns at the bow area

(b) Icebreaking patterns at the stern area

Fig. 15. Comparisons of the icebreaking progress during ship-ice interaction between laboratory photographs (Jeong et al., 2017) (left) and SPH particle snapshots (right) (contours of accumulated plastic strain).

open channel appears after the ship model ran through the level ice. However, because water was not taken into account in the SPH simulation, there were no broken ice pieces floating in the open channel after the ship ran with high speed $V = 0.6$ m/s. This case can demonstrate the effectiveness of the SPH for modeling the

failure of the ice. The water phase will be considered in the future study.

Fig. 15 shows the comparison of the detailed ice failure pattern and the movement of broken ice floes between the numerical results and pictures in model test (Jeong et al., 2017). The model scale $\lambda = 18.667$, ice thickness $H = 0.06$ m and the ship velocity $V = 0.357$ m/s are used in this model test. When the ship moves and interacts with the ice sheet, localised crushing of ice occurs at the bow stem and increases at the contact area as the ship advances until ice fails by bending downwards around either side of the bow in Fig. 15(a). It can be seen in both results of numerical simulation and model-scale test in Fig. 15(a), the broken ice floes submerge under the bow and slid along the hull at the bow area. Correspondingly, the bow is fully covered by broken ice floes underwater. In addition, it can also be observed that there is no accumulation and pile up of broken ice floes in front of the ship model.

It can be seen in Fig. 15(b), some local crushing events also occur on the port and starboard side of the hull. It also shows some large ice pieces are bent down from the level ice on the both side of the mid-hull in Fig. 15(b). Then most broken ice pieces are pushed laterally by the hull and few broken ice pieces emerge in the open channel that is created behind the ship both in the numerical and experimental results. It can be observed that just few large ice pieces slide on the bottom of the hull at the stern area in the numerical simulation, which is different with that in picture of model test where lots of broken ice pieces slide under the bottom of the hull at the either side of stern. In addition, it can be found that some broken ice pieces move laterally below the bordering ice sheet in the test result. However, this phenomenon does not exist in our simulations. The main reason for these differences may be that the real effect of water is not considered enough in our simulation. The neglect of propeller may also account for these differences partly.

The above comparisons show that the presented SPH model can give similar trend of the interaction process of level ice and ship with that in the model-scale test, although there are some differences in details. It implies that the present SPH model can be used effectively for simulating the ice failure process during ice-ship interactions.

Fig. 16 shows the equivalent stress distribution for the level ice during the interaction progress with ship. It can be found that the ice breaking process is not always symmetric at both sides, which is reasonable and also reported in Zhou et al. (2018a). It should be noted that because the edges of level lice, except the one interacting with ship, are fixed and free of deformation, there are slight stress changes on at both side edges of the ice plate in Fig. 16.

To quantitatively illustrate the accuracy of the SPH, the time histories of the ice breaking resistance are shown in Fig. 17. It is found that the ice resistances predicted by the SPH method is generally stable, although there exist some oscillations, which are reasonable due to the sliding and covering of broken ice pieces on bottom of ship hull. In general, the ice breaking resistance increases with larger ship velocity. In addition, for the same ship velocity, the corresponding ice breaking resistance increases with thicker level ice.

Fig. 18 illustrates the comparison of the ice breaking resistance against the ship velocities between the experimental data (Lau and Akinturk, 2011) and the SPH results. The results of SPH in Fig. 18 are obtained by averaging the corresponding ice resistance in Fig. 17 after $t = 4.0$ s, where the ice breaker has completely entered into the level ice and the resistance becomes stable. In general, the ice resistance becomes larger with the icebreaker speed increasing, of which the trends are in good agreement with the model test, even though there are some differences and the presented SPH model overestimates the ice breaking resistance. The main reason may be that the real effect of water is not considered, and the crushed ice
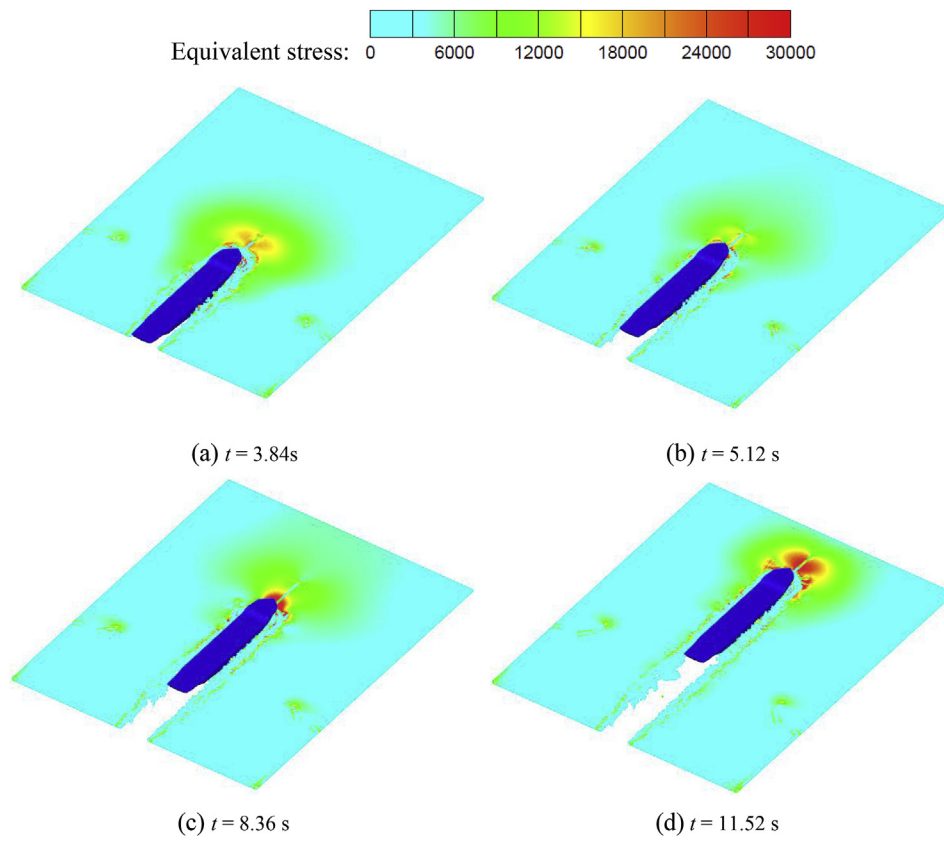
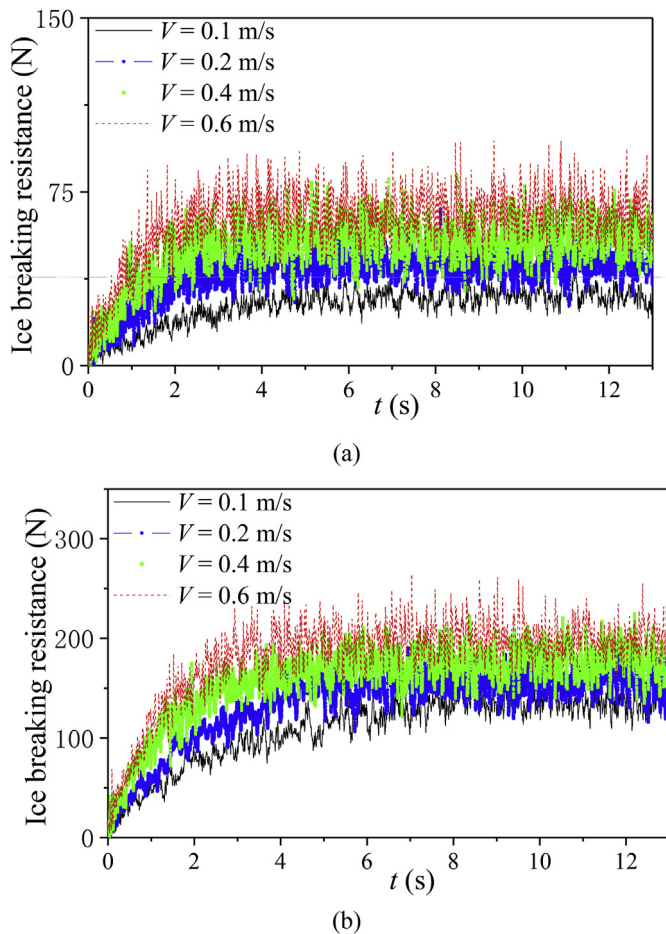Fig. 16. The equivalent stress distribution for the level ice.

Fig. 17. Ice breaking resistance time history in terms of different ship velocities. (a) $H = 0.04$ m; (b) $H = 0.06$ m.
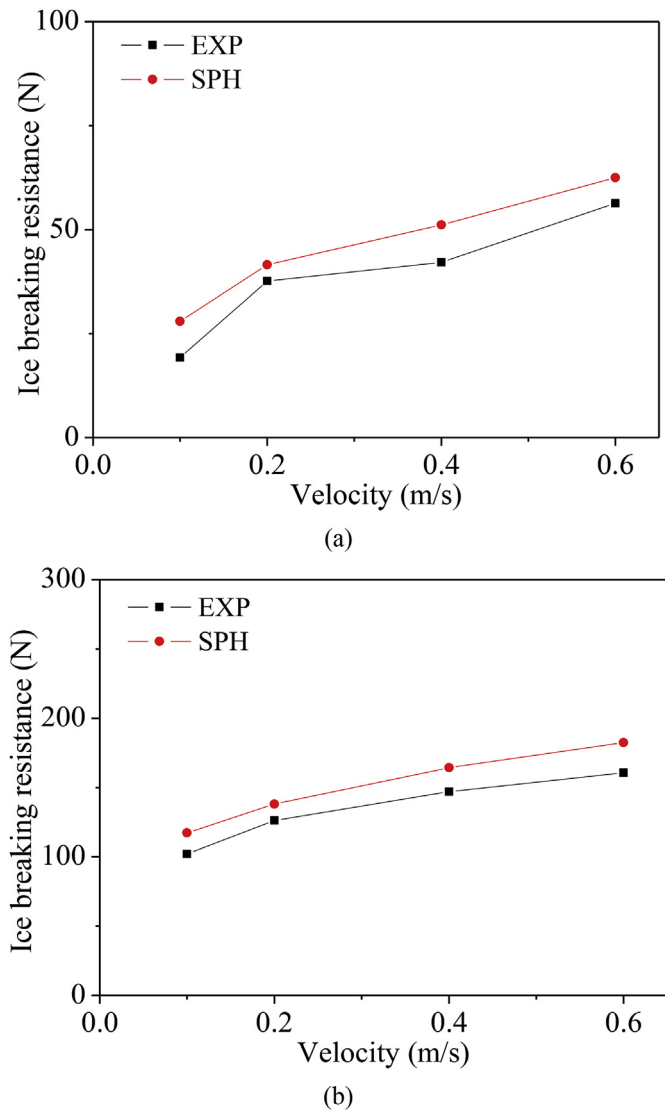

Fig. 18. Comparison of ice breaking resistance in terms of different ship velocities between SPH results and laboratory data. (a) $H = 0.04$ m; (b) $H = 0.06$ m.

always slide and cover around the bottom of icebreaker, which may cause ice breaking resistance to be larger than experimental data. In addition, the uneven distribution of ice properties in nature may also partially contribute to the differences.

6. Conclusions

In this paper, the SPH model including the elastic-plastic cohesion softening model is proposed to simulate the ice failure and ice breaking process of icebreaker in the level ice. The predicted stress-strain curve and stress time history in three-point bending failure test are in good agreement with the experimental results, and the simulated failure process of ice against sloping structure by using the present SPH model are qualitatively reasonable and acceptable. Besides, the conducted studies disclosed that the elastoplastic cohesion softening Drucker-Prager failure model can be effectively used to simulate the failure process of ice. In addition, the good agreement between the results of the SPH and the experimental data for simulating the ice-ship interaction indicates that the performance of SPH is satisfactory in view of accuracy and stability, although there is still a space for improvement. Future work is needed to include the water phase to simulate more complex ice-structure and ice-ship-water interactions.

References

Adami, S., Hu, X.Y., Adams, N.A., 2012. A generalized wall boundary condition for smoothed particle hydrodynamics. J. Comput. Phys. 231 (21), 7057—7075.
Aksnes, V., 2010. A simplified interaction model for moored ships in level ice. Cold

Reg. Sci. Technol. 63 (1), 29–39.

Benz, W., Asphaug, E., 1995. Simulations of brittle solids using smooth particle hydrodynamics. Comput. Phys. Commun. 87, 253–265.

Bouscasse, B., Colagrossi, A., Marrone, S., Antuono, M., 2013. Nonlinear water wave interaction with floating bodies in sph. J. Fluid Struct. 42 (4), 112–129.

Bui, H., Fukagawa, R., Sako, K., Ohno, S., 2008. Lagrangian meshfree particles method (SPH) for large deformation and failure flows of geomaterial using elastic–plastic soil constitutive model. Int. J. Numer. Anal. Methods Geomech. 32 (12), 1537–1570.

Cho, S.R., Jeong, S.Y., Lee, S., 2013. Development of effective model test in pack ice conditions of square-type ice model basin. Ocean Eng. 67 (67), 35–44.

Cho, S.R., Lee, S., 2015. A prediction method of ice breaking resistance using a multiple regression analysis. Int. J. Nav. Arch. Ocean. 7 (4), 708–719.

Deb, D., Pramanik, R., 2013. Failure process of brittle rock using smoothed particle hydrodynamics. J. Eng. Mech. 139 (11), 1551–1565.

Eghtesad, A., Shafiei, A.R., Mahzoon, M., 2012. A new fluid–solid interface algorithm for simulating fluid structure problems in fgm plates. J. Fluid Struct. 30 (2), 141–158.

Gao, Y., Hu, Z., Ringsberg, J.W., Wang, J., 2015. An elastic–plastic ice material model for ship-iceberg collision simulations. Ocean Eng. 102, 27–39.

Gotoh, H., Khayyer, A., 2018. On the state-of-the-art of particle methods for coastal and ocean engineering. Coast Eng. J. 60 (1), 79–103.

Gray, J., Monaghan, J., Swift, R., 2001. SPH elastic dynamics. Comput. Methods Appl. Mech. Eng. 190 (49–50), 6641–6662.

Hu, J., Zhou, L., 2015. Experimental and numerical study on ice resistance for ice-breaking vessels. Int. J. Nav. Arch. Ocean. 7 (3), 626–639.

Jeong, S.Y., Choi, K., Kang, K.J., Ha, J.S., 2017. Prediction of ship resistance in level ice based on empirical approach. Int. J. Nav. Arch. Ocean. 9 (6).

Ji, S.Y., Wang, A.L., Su, J., Yue, Q.J., 2011. Experimental studies on elastic modulus and flexural strength of sea ice in the bohai sea. J. Cold Reg. Eng. 25 (4), 182–195.

Jordaan, I.J., 2001. Mechanics of ice–structure interaction. Eng. Fract. Mech. 68 (17), 1923–1960.

Keinonen, A.J., Browne, R., Revill, C., Reynolds, A., 1996. Icebreaker Characteristics Synthesis, Report TP 12812E. The Transportation Development Centre, Transport Canada, Ontario.

Khayyer, A., Gotoh, H., Falahaty, H., Shimizu, Y., 2018. An enhanced isph-sph coupled method for simulation of incompressible fluid-elastic structure interactions. Comput. Phys. Commun. 232, 139–164.

Khayyer, A., Gotoh, H., Shimizu, Y., Gotoh, K., Shao, S., 2017. An enhanced particle method for simulation of fluid flow interactions with saturated porous media. Journal of JSCE Ser B2 73 (2), I_841–I_846.

Lau, M., Akinturk, A., 2011. KORDI Araon Model Tests in Ice Using the Planar Motion Mechanism, Report LM-2011-04. Canada: St. John's, Newfoundland and Labrador. National Research Council – Institute for Ocean Technology.

Libersky, L.D., Petschek, A.G., 1991. Smoothed particle hydrodynamics with strength of materials. In: Trease, H., Friits, J., Crowley, W. (Eds.), Proceedings of the Next Free Lagrange Conference, vol. 395. Springer, New York, pp. 248–257.

Lindqvist, G., 1989. A straightforward method for calculation of ice resistance of ships. The 10th International Conference on Port and Ocean Engineering Under Arctic Conditions 2, 722–735.

Liu, R.W., Xue, Y.Z., Lu, X.K., Cheng, W.X., 2018. Simulation of ship navigation in ice rubble based on peridynamics. Ocean Eng. 148, 286–298.

Long, S.Y., 2014. Meshless Methods and Their Applications in Solid Mechanics. Science Press, Beijing, China, pp. 235–238.

Lubbad, R., Løset, S., 2011. A numerical model for real-time simulation of ship-ice interaction. Cold Reg. Sci. Technol. 65, 111–127.

Lu, W.J., Serre, N., Høyland, K.V., Evers, K.U., 2013. Rubble Ice Transport on Arctic Offshore Structures (RITAS), part IV: tactile sensor measurement of the level ice load on inclined plate. In: Proceedings of the 22nd International Conference on Port and Ocean Engineering under Arctic Conditions, Espoo, Finland.

Ma, Q.W., 2008. A new meshless interpolation scheme for MLPG_R method. CMES-Comput. Model. Eng. Sci. 23 (2), 75–89.

Matlock, H., Dawkins, W.P., Panak, J.J., 1969. A model for the prediction of ice-structure interaction. In: Annual Offshore Technology Conference, Dallas, USA, pp. 687–694.

Monaghan, J.J., Lattanzio, J.C., 1985. A refined particle method for astrophysical problems. Astron. Astrophys. 149 (149), 135–143.

Monaghan, J.J., 1992. Smoothed particle hydrodynamics. Annu. Rev. Astron. Astro-phys. 30, 543–574.

Monaghan, J.J., 2000. SPH without a tensile instability. J. Comput. Phys. 159 (2), 290–311.

Morris, J., Fox, P., Zhu, Y., 1997. Modeling low Reynolds number incompressible flows using SPH. J. Comput. Phys. 136 (1), 214–226.

Paavilainen, J., Tuhkuri, J., Polojarvi, A., 2011. 2D numerical simulation of ice rubble formation process against an inclined structure. Cold Reg. Sci. Technol. 68 (1–2), 20–34.

Randles, P., Libersky, L., 1996. Smoothed particle hydrodynamics: some recent improvements and applications. Comput. Methods Appl. Mech. Eng. 139 (1), 375–408.

Schulson, E.M., 1997. The brittle failure of ice under compression. J. Phys. Chem. B 101 (32), 6254–6258.

Schulson, E.M., 2001. Brittle failure of ice. Eng. Fract. Mech. 68 (17), 1839–1887.

Schulson, E.M., Duval, P., 2009. Creep and Fracture of Ice. Cambridge University Press, Cambridge, UK.

Shao, S.D., Lo, E.Y.M., 2003. Incompressible SPH method for simulating Newtonian and non-Newtonian flows with a free surface. Adv. Water Resour. 26 (7), 787–800.

Shi, Y., Li, S.W., Chen, H.B., He, M., Shao, S.D., 2018. Improved SPH simulation of spilled oil contained by flexible floating boom under wave–current coupling condition. J. Fluid Struct. 76, 272–300.

Su, B., Riska, K., Moan, T., 2010. A numerical method for the prediction of ship performance in level ice. Cold Reg. Sci. Technol. 60, 177–188.

Swegle, J., Hicks, D., Attaway, S., 1995. Smoothed particle hydrodynamics stability analysis. J. Comput. Phys. 116 (1), 123–134.

Valanto, P., 2001. The resistance of ships in level ice. SNAME Transactions 109, 53–83.

Withalm, M., Hoffmann, N.P., 2010. Simulation of full-scale ice-structure-interaction by an extended Matlock-model. Cold Reg. Sci. Technol. 60, 130–136.

Zhang, N.B., Zheng, X., Ma, Q.W., 2017. Updated smoothed particle hydrodynamics for simulating bending and compression failure progress of ice. Water 9 (11), 882.

Zheng, X., Ma, Q.W., Duan, W.Y., 2014. Incompressible SPH method based on Rankine source solution for violent water wave simulation. J. Comput. Phys. 276, 291–314.

Zheng, X., Shao, S.D., Khayyer, A., Duan, W.Y., Ma, Q.W., Liao, K.P., 2017. Corrected first-order derivative ISPH in water wave simulations. Coast Eng. J. 59 (1), 1750010.

Zhou, L., Chuang, Z., Ji, C., 2018a. Ice forces acting on towed ship in level ice with straight drift. part I: analysis of model test data. Int. J. Nav. Arch. Ocean. 10 (1), 60–68.

Zhou, L., Chuang, Z., Ji, C., 2018b. Ice forces acting on towed ship in level ice with straight drift. part II: numerical simulation. Int. J. Nav. Arch. Ocean. 10 (2), 119–128.

Zhou, L., Riska, K., Moan, T., Su, B., 2013. Numerical modeling of ice loads on an icebreaking tanker: comparing simulations with models tests. Cold Reg. Sci. Technol. 87 (3), 33–46.

Zhou, Q., Peng, H., Qiu, W., 2016. Numerical investigations of ship-ice interaction and maneuvering performance in level ice. Cold Reg. Sci. Technol. 122, 36–49.